Statistical model of short wavelength transport through cavities with coexisting chaotic and regular ray trajectories

Ming-Jer Lee, Thomas M. Antonsen, and Edward Ott

Phys. Rev. E **87**, 062906 — Published 13 June 2013

DOI: 10.1103/PhysRevE.87.062906

Statistical Model of Short Wavelength Transport Through Cavities with Coexisting Chaotic and Regular Ray Trajectories

Ming-Jer Lee,* Thomas M. Antonsen, and Edward Ott
University of Maryland, College Park, Maryland 20742, USA

We study the statistical properties of the impedance matrix (related to the scattering matrix) describing the input/ouput properties of waves in cavities in which ray trajectories that are regular and chaotic coexist (i.e., 'mixed' systems). The impedance can be written as a summation over eigenmodes where the eigenmodes can typically be classified as either regular or chaotic. By appropriate characterizations of regular and chaotic contributions, we obtain statistical predictions for the impedance. We then test these predictions by comparison with numerical calculations for a specific cavity shape, obtaining good agreement.

I. INTRODUCTION

In principle, for a given configuration, properties of wave systems are completely determined, and thus are not random. However, at short wavelength, these properties can be very sensitively dependent on small configurational changes or changes of the free space wavelength. If the configuration or free space wavelength is regarded as slightly uncertain within some small range and the wave properties vary wildly in this range, then a statistical approach may be warranted. This type of approach was originally introduced by E. Wigner in reference to the energy levels of large nuclei [1–3], and later employed to study classically chaotic quantum systems [2, 4]. Here we focus on quasi-two-dimensional microwave cavities and quantum dots which couple to an external environment through suitable openings (called 'leads' or 'ports'). The statistical properties in chaotic cavities with external connections have been well studied using various approaches, e.g., the 'Poisson Kernel' [5, 6] or the 'Random Coupling Model' (RCM) [7]. The RCM (employed in the present paper) focuses on impedance matrices (related to scattering matrices through an elementary transformation) and replaces the eigenfunctions and eigenenvalues in the impedance formula by suitably choosen random quantities. Past work has shown that the RCM, and ,equivalently, the Poisson Kernel yield results that agree well with statistical data obtained from experiments and numerical computations on microwave cavities [6, 8–10]. However, in general, such systems may have not only either all chaotic or all regular orbits, but also typically have a mixture of coexisting chaotic and regular orbits. We called such systems 'mixed'. The statistical properties of impedance matrices in mixed systems is the subject of this paper.

For specificity we focus on a particular mixed system, a 'mushroom' cavity (Fig. 1(a)) [11], which has a clearly divided phase space [12]. For most modes of this system, we find that it is possible to separate them into two classes, regular and chaotic (this may not hold for other systems). Using this separation, we decompose the impedance formula into chaotic and regular parts. We then derive the probability distribution associated with the chaotic part of the impedance, while, for the regular part we utilize exact (numerically calculated) or approximate theoretical eigenmodes. To test our theory, we numerically solve for eigenvalues and eigenfunctions of our mushroom cavity and insert them into the exact formula.

This paper is organized as follows. In Sec. II we review the impedance formula in two dimensional cavities, introduce the random coupling model, generalize the RCM to mixed systems, introduce the mushroom cavity (an example of a mixed system), and apply our generalized RCM to this cavity. In Sec. III we numerically calculate the impedance matrix of the mushroom cavity and compare the numerical results with results from our statistical theory. Conclusions and discussion are presented in Sec. IV.

The general problem of wave properties of systems whose ray equations have a mixed phase space was first addressed by Berry and Robnik [13] who studied the spectra of mixed closed systems. Subsequently, many other researchers have investigated spectra and wavefunctions of closed systems with mixed ray orbit phase space (e.g., [14, 15]). The problem of characterizing the input/output properties of mixed open systems, however, has, to our knowledge, been addressed relatively little [16–18].

II. REVIEW OF THEORY

A. Impedance of a cavity

In the presentation that follows, we consider the context of electromagnetic waves. However, we emphasized that, with appropriate notational changes, these considerations apply equally well to quantum waves, acoustic waves, elastic waves, etc.

We consider a vacuum-filled, quasi-two-dimensional (vertically thin) microwave cavity with cavity height h and M ports as shown in Fig. 1. We denote the two dimensional interior of the cavity by $\Omega \in \mathbb{R}^2$. If the frequency is not too high (i.e., the wavelength is greater than $2h$), then only vertical electric fields are excited in-

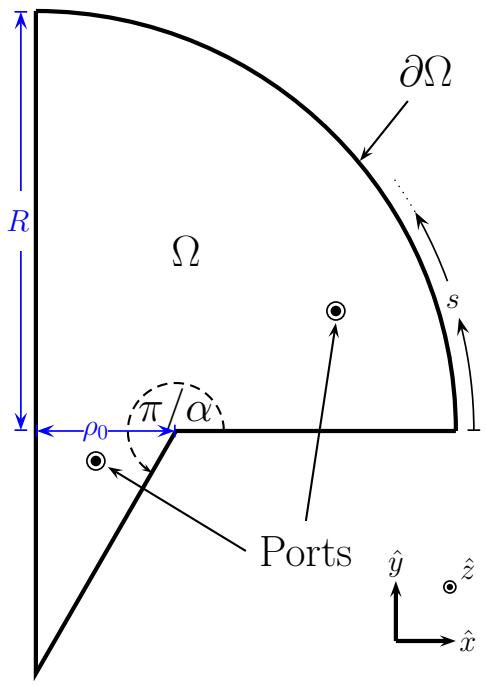

(a)

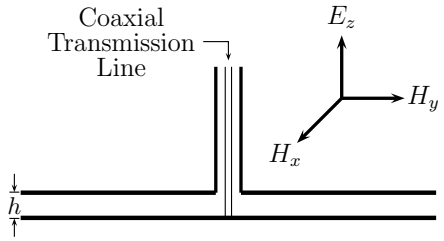

(b)

FIG. 1. (a) Top view of the quasi-two dimensional cavity coupling with $M = 2$ ports (fed by coaxial transmission lines), where the region interior to the cavity is denoted Ω. (b) Sideview of the cavity at a port. In some previous works, a mushroom billiard similar to that in (a) was used [11], but the billiard section below the quarder circular cap being a rectangle of width ρ_0. This, however, introduced neutrally stable ray orbits that bounce back and forth horizontally between the vertical walls of the rectangle. By using the above triangular bottom part (as in Ref. [19]) (a) we avoid the non-generic effects of such orbits.

side the cavity,

$$\vec{E} = E_z(\vec{x}, t)\hat{z}, \tag{1}$$

where $\vec{x} \in \Omega$ is a two dimensional position vector. The surface charge density on the bottom plate of such a cavity is $\rho_s = -\epsilon_0 E_z$, and the voltage difference between the two plates is

$$V_T(\vec{x}, t) = hE_z(\vec{x}, t). \tag{2}$$

The surface current density on the bottom plate is related to the magnetic field, $\vec{H}$, which is perpendicular to $\vec{E}$, by

$$\vec{J}_s = \vec{H} \times \hat{z}. \tag{3}$$

We assume that the fields are excited by M localized current sources, which inject surface charge density on the bottom plate

$$\dot{\rho}_s(\vec{x}, t) = \sum_{j=1}^{M} I_j(t) u_j(\vec{x}), \tag{4}$$

where $u_j(\vec{x})$ is the normalized profile function of port j, $\int d^2\vec{x} u_j(\vec{x}) = 1$, and we regard Eq. (4) as modeling the currents induced by the transmission line fed ports shown in Fig. 1. With Eq. (3), the continuity equation for the surface charge can be written as

$$\frac{\partial}{\partial t}(-\epsilon_0 E_z) + \vec{\nabla} \cdot (\vec{H} \times \hat{z}) = \dot{\rho}_s = \sum_{j=1}^{M} I_j u_j. \tag{5}$$

Differentiating Eq. (5), using Faraday's law, $\nabla \times \vec{E} = -\mu_0 \partial \vec{H}/\partial t$, and expressing E_z by Eq. (2), we obtain

$$\frac{1}{c^2}\frac{\partial^2}{\partial t^2} V_T - \nabla^2 V_T = h\mu_0 \sum_{j=1}^{M} u_j \frac{\partial}{\partial t} I_j, \tag{6}$$

where $c = 1/\sqrt{\mu_0 \epsilon_0}$ is the speed of light. Assuming that $V_T(\vec{x}, t) = \hat{V}_T(\vec{x}) e^{j\omega t}$, $I_i(t) = \hat{I}_i e^{j\omega t}$, Eq. (6) can be rewritten as

$$(\nabla^2 + k^2)\hat{V}_T = -jkh\eta_0 \sum_{j=1}^{M} u_j \hat{I}_j, \tag{7}$$

where $k = \omega/c$, and $\eta_0 = \sqrt{\mu_0/\epsilon_0}$ is the free space impedance.

We expand $\hat{V}_T$ in the basis of the eigenfunctions of the closed cavity, i.e.,

$$\hat{V}_T = \sum_{n=1}^{\infty} c_n \phi_n, \tag{8}$$

where ϕ_n satisfies the Helmholtz equation with Dirichlet boundary condition and a proper normalization condition, i.e.,

$$(\nabla^2 + k_n^2)\phi_n(\vec{x}) = 0 \quad \vec{x} \in \Omega, \tag{9}$$

$$\phi_n(\vec{x}) = 0 \quad \vec{x} \in \partial\Omega, \tag{10}$$

$$\int_\Omega \phi_i \phi_j d^2\vec{x} = \delta_{ij}, \tag{11}$$

and we order the mode labeling according to the convention, $k_{n+1}^2 \geq k_n^2$. Inserting Eq. (8) into Eq. (7), multiplying $\phi_m(\vec{x})$ and integrating over Ω, we obtain

$$c_m = -jkh\eta_0 \sum_{j=1}^{M} \frac{\langle u_j \phi_m \rangle \hat{I}_j}{k^2 - k_m^2}, \tag{12}$$

where $\langle \cdots \rangle \equiv \int_\Omega \cdots d^2\vec{x}$. The voltage at port i is defined as

$$\hat{V}_i = \langle u_i \hat{V}_T \rangle, \tag{13}$$

where the port voltages V_i are expressed in phaser form, $V_i = \hat{V}_i e^{j\omega t}$. Using Eqs. (8), (12) and (13), we obtain

$$\hat{V}_i = \sum_{j=1}^{M} Z_{ij} \hat{I}_j, \tag{14}$$

where the i, j element of the impedance matrix $\mathbf{Z}$ is given by

$$Z_{ij} = -jkh\eta_0 \sum_{n=1}^{\infty} \frac{\langle u_i \phi_n \rangle \langle u_j \phi_n \rangle}{k^2 - k_n^2}. \tag{15}$$

Equation (15) states that, in a lossless cavity, the impedance is purely imaginary, since the eigenfunctions for Eqs. (9) and (10) are real. It also states that, if we know all the eigenfunctions and eigenvalues of the closed cavity, we can calculate the matrix elements of $\mathbf{Z}$ exactly. Note that $\langle u_i \phi_n \rangle \to 0$ as the port size becomes much greater than several wavelengths. Thus, the infinite sum in Eq. (15) can be replaced by a finite sum, i.e.,

$$Z_{ij} = -jkh\eta_0 \sum_{n=1}^{N} \frac{\langle u_i \phi_n \rangle \langle u_j \phi_n \rangle}{k^2 - k_n^2}, \tag{16}$$

where N satisfies the condition, $2\pi/k_N \ll$ (size of ports). For systems that are large compared to a wavelength $(2\pi/k)$ and may have some uncertainty in their specification, it is often of practical interest to dispense with the neccessity of numerically calculating all N eigenfunctions and to instead look for a statistical description. The later will be our goal.

B. Random Coupling Model

The Random Coupling Model (RCM) treats the case where typical ray orbits are *all* chaotic and is based on the supposition that, in the short wavelength limit, the statistical properties of the impedance of a chaotic cavity can be obtained from Eq. (16) by replacing k_n^2 and $\langle u_i \phi_n \rangle$ by suitable random variables.

According to the Weyl's formula [20] for a two dimensional cavity of area A, the mean spacing between two adjacent eigenvalues, $k_n^2 - k_{n-1}^2$, is $4\pi/A$, i.e.,

$$\Delta \equiv \langle k_n^2 - k_{n-1}^2 \rangle = \frac{4\pi}{A}. \tag{17}$$

References [1, 2, 21] state that the normalized eigenvalue spacing, $s_n \equiv (k_n^2 - k_{n-1}^2)/\Delta$, of a time-reversible chaotic system has similar statistical properties to the spacings of the eigenvalues of large matrices randomly drawn from the Gaussian Orthogonal Ensemble (GOE) of random matrices with unit mean eigenvalue spacing. In this paper, our eigenfunctions are always real, as appropriate to time reversible systems, and, henceforth, GOE is automatically assumed when we mention random matrices.

Berry [22] argues that the wavefunction at any point in a chaotic billiard has similar statistical properties to a random superposition of many plane waves,

$$\phi_n(\vec{x}) \approx \mathrm{Re}\left\{ \sum_{j=1}^{J} \alpha_j \exp\left(ik_n \vec{e}_j \cdot \vec{x} + i\beta_j\right) \right\}, \quad J \gg 1, \tag{18}$$

where it is assumed that $\vec{x}$ is not too close to the billiard boundary, the wavenumber k_n is fixed, but propagation directions $\vec{e}_j$, amplitudes α_j, and phases β_j are random variables. To be more specific, directions and phases are uniformly distributed in $[0, 2\pi]$, and all amplitudes have the same distribution. By the central limit theorem, for $J \gg 1$, $\phi_n(\vec{x})$ evaluated at the point $\vec{x}$ is a Gaussian random variable with zero mean, and its variance can be determined by the normalization condition, i.e.,

$$\int_\Omega \phi_n^2 d^2\vec{x} = 1, \tag{19}$$

which implies

$$\mathrm{E}\{\phi_n^2\} = 1/A. \tag{20}$$

The probability distribution function of the overlap integral $\langle u_i \phi_n \rangle$ is Gaussian with expectation value zero (since ϕ_n is a Gaussian with expection value zero), and by Eq. (18) the variance of $\langle u_i \phi_n \rangle$ is

$$\mathrm{E}\{\langle u_i \phi_n \rangle^2\} = \frac{1}{A} \int_0^{2\pi} \frac{d\theta}{2\pi} |\bar{u}(\vec{k}_n)|^2, \tag{21}$$

where $\vec{k}_n = (k_n \cos\theta, k_n \sin\theta)$, and $\bar{u}(\vec{k}_n)$ is the Fourier transform of the profile function $u(\vec{x})$,

$$\bar{u}(\vec{k}_n) = \int d^2\vec{x} u(\vec{x}) \exp\left(-i\vec{k}_n \cdot \vec{x}\right). \tag{22}$$

Note that, the variance of $\langle u_i \phi_n \rangle$ depends on the eigenvalue k_n^2 through Eq. (22) where $|\vec{k}_n| = k_n$. If $2\pi/k_n \gg$ (size of the port), the profile function of the port can be approximated by a delta function, i.e., $\langle u_i \phi_n \rangle = \phi_n(\vec{x}_i)$; if $2\pi/k_n$ is comparable to the port size, we need to consider the variations of ϕ_n over the ports. Eventually, for short enough wavelength we have $\mathrm{E}\{\langle u_i \phi_n \rangle\} \to 0$ as $k_n \to \infty$.

For an M port system, we need to consider the same wavefunction at different positions; e.g., if $2\pi/k \gg$ (size of the port), for two ports located at $\vec{x}_i$ and $\vec{x}_j$, we need to consider $\langle u_i \phi_n \rangle \cong \phi_n(\vec{x}_i)$ and $\langle u_j \phi_n \rangle \cong \phi_n(\vec{x}_j)$, which are not, in general, independent, although independence can be approximately assumed if the ports are many wavelengths apart. In the RCM, we build in this relation by writing

$$\Phi_n \equiv [\langle u_1 \phi_n \rangle, \ldots, \langle u_M \phi_n \rangle]^T = \frac{1}{\sqrt{A}} \mathbf{w}_n, \tag{23}$$

where the $1/\sqrt{A}$ factor is based on the expectation value of ϕ_n^2, and $\mathbf{w}_n (n = 1, 2, \ldots, N)$ is an M-dimensional, zero mean, standard Gaussian random vectors whose covariance matrix may have nonzero non-diagonal elements reflecting correlation between nearby ports. We can rewrite the impedance matrix as

$$\mathbf{Z} = -jkh\eta_0 \frac{\Delta}{4\pi} \sum_{n=1}^{N} \frac{\mathbf{w}_n \mathbf{w}_n^T}{k^2 - k_n^2}. \tag{24}$$

where we have used Eq. (17) to replace A.

In the case of identical transmission line inputs that are far enough apart, we can neglect correlations between the ports and the covariance matrix of $\mathbf{w}_n$ is $\mathbf{1}_{M\times M}$; i.e., $E(w^i w^j) = \delta_{ij}$ for $i, j = 1, 2, \ldots, M$. In this case, we introduce the normalized reactance matrix,

$$\mathbf{\Xi} = -\frac{1}{\pi} \sum_n \frac{\mathbf{w}_n \mathbf{w}_n^T}{\tilde{k}^2 - \tilde{k}_n^2}, \tag{25}$$

where $\tilde{k}^2 = k^2/\Delta$ and the mean spacing, $\tilde{k}_n^2 - \tilde{k}_{n-1}^2$, between normalized eigenvalues is one. In this case the impedance matrix becomes

$$\mathbf{Z} = j\frac{kh\eta_0}{4}\mathbf{\Xi}. \tag{26}$$

Note that the normalized reactance matrix, $\mathbf{\Xi}$, is independent of all system specific information, such as the cavity shape, area, etc.; namely, it is universal for all chaotic cavities with widely separated ports.

C. Impedance in Mixed Systems

For a generic two dimensional billiard, both regular and chaotic phase space regions coexist, and we call such a system mixed. Percival's conjecture [23] states that semiclassical eigenmodes in mixed systems live either in regular or chaotic regions. Our numerical computations support this conjecture (see Fig. 2). At short wavelength, the number of regular and chaotic eigenstates can be approximately counted by the Partial Weyl law [24],

$$\bar{N}_\Gamma(k^2) = \frac{A_\Gamma}{4\pi}k^2 + O(k), \tag{27}$$

where $\Gamma = R$ denotes regular trajectories and $\Gamma = C$ denotes chaotic trajectories, A_Γ/A is the ratio of the phase space volume occupied by Γ, and A_Γ is given by

$$A_\Gamma = \int_\Omega d^2\vec{x} \frac{1}{2\pi} \int_0^{2\pi} d\theta \zeta_\Gamma(\vec{x}, \theta). \tag{28}$$

Here, $\zeta_\Gamma(\vec{x}, \theta)$ is the characteristic function of Γ at $(\vec{x}, \theta)$, i.e., $\zeta_\Gamma(\vec{x}, \theta) = 1$ if the trajectory running through $\vec{x}$ at θ angle belongs to Γ and $\zeta_\Gamma(\vec{x}, \theta) = 0$, otherwise.

Following the above approach, we decompose (16) into the contributions $\mathbf{Z}_R$ and $\mathbf{Z}_C$ to the impedance from the regular eigenmodes and chaotic eigenmodes, as follows,

$$\mathbf{Z} = \mathbf{Z}_R + \mathbf{Z}_C, \tag{29a}$$

and

$$Z_{R,ij} = -jkh\eta_0 \sum_r^{N_R} \frac{\langle u_i \phi_r \rangle \langle u_j \phi_r \rangle}{k^2 - k_r^2}, \tag{29b}$$

$$Z_{C,ij} = -jkh\eta_0 \sum_c^{N_C} \frac{\langle u_i \phi_c \rangle \langle u_j \phi_c \rangle}{k^2 - k_c^2}, \tag{29c}$$

where $\phi_r(\phi_c)$ denotes regular (chaotic) wavefunctions, $r = 1, 2, \ldots, N_R (c = 1, 2, \ldots, N_C)$, and $N_R + N_C = N$.

The semiclassical wavefunction distribution for chaotic eigenfunctions in mixed systems can be described by the so-called Restricted Random Wave Model [25],

$$P_{\vec{x}}(\phi) = \frac{1}{\sqrt{2\pi\sigma^2(\vec{x})}} \exp\left[-\frac{\phi^2}{2\sigma^2(\vec{x})}\right], \tag{30}$$

where

$$\sigma^2(\vec{x}) = \frac{1}{2\pi A_C} \int_0^{2\pi} d\theta \zeta_C(\vec{x}, \theta). \tag{31}$$

In a two dimensional pure chaotic cavity, $\sigma^2 = 1/A$ is independent of $\vec{x}$.

The statistics of k_c^2 in mixed systems is hypothesized to be similiar to the statistics of k_n^2 in chaotic systems, but the mean of the spacing between chaotic eigenvalues, $k_{c+1}^2 - k_c^2$, is given by $4\pi/A_C$, as opposed to $4\pi/A$ in the purely chaotic case. Thus, the statistics of the chaotic normalized reactance in mixed systems should be identical to the statistics of the normalized reactance in chaotic systems.

We do not expect to find explicit universal statistics for the regular eigenfunctions ϕ_r as they are dependent on the cavity shape. However, the regular normalized reactance in mixed systems is always Lorentzian distributed (see Appendix A).

D. Mushroom Billiard

The mushroom billiard [11, 26] was first introduced by Bunimovich. Since the cap of the mushroom is a quarter circle, there are orbits that never leave the cap region and are the same as the orbits in a complete quarter circle billiard having the same radius R (see Fig. 2(a)). These orbits are tangent to a circular caustic with a radius C_r. If the caustic radius $C_r > \rho_0$, (see Fig. 1) this orbit is trapped in the cap, and is integrable. There are also chaotic orbits that travel throughout the whole billiard (Fig. 2(b)), visiting both the cap region and the triangular region below the cap. Thus, the mushroom billiard is an example of a mixed system.

The eigenmodes of the Helmholtz equation in a quarter circle with radius R can be described by two quantum number, $(m, n) \leftrightarrow r$, and the corresponding eigenfunction is

$$\phi_r \cong \phi_{mn}^{(0)}(\rho, \theta) = \mathcal{N}_{mn} J_m(k_{mn}\rho) \sin m\theta, \tag{32}$$

with normalization constant

$$\mathcal{N}_{mn} = \frac{2\sqrt{2}}{\sqrt{\pi} R J'_m(k_{mn}R)}, \tag{33}$$

and $\phi^{(0)}_{mn} \equiv 0$ outside the quarter circle. Here J_m is m-th order Bessel function of the first kind, k_{mn} is the eigenwavenumber such that $k_{mn}R$ is the n-th zero of J_m.

To relate the quantum eigenmodes to the classical motion [27], we first define the classical probability distribution for position ρ,

$$P_{CL}(\rho) = \frac{\rho}{\sqrt{R^2 - C_r^2}\sqrt{\rho^2 - C_r^2}}, \tag{34}$$

where $P_{CL}(\rho)d\rho$ represents the fraction of time a classical trajectory spends in the interval $d\rho$ at ρ, $R > \rho > C_r$. The classical caustic radius C_r is defined in terms of the angle of incidence ϕ that the trajectory makes with respect to the boundary at R, $C_r/R = \sin\phi$. The analogous caustic radius C_r from the wavefunction (32) is identified by equating the Bessel function order to its argument,

$$C_r = R_{mn} \equiv \frac{m}{k_{mn}} R. \tag{35}$$

For eigenmodes with $R_{mn} < \rho_0$, the classical orbit in the full, quarter-circle billiard will travel to the root of the mushroom so the orbit in the mushroom is no longer integrable, and the corresponding $\phi^{(0)}_{mn}$ modes in (32) are not present in our system. Thus, we can approximate (29b) using the quarter circle eigenfunctions $\phi^{(0)}_{mn}$ given by Eq. (32),

$$Z_{ij,R} = -jkh\eta_0 \sum_{\substack{m,n \\ \rho_0 < R_{mn} < R}} \frac{\langle u_i \phi^{(0)}_{mn}\rangle \langle u_j \phi^{(0)}_{mn}\rangle}{k^2 - k^2_{mn}}. \tag{36}$$

In order to apply the RCM for the chaotic contribution to the mushroom cavity, we need the statistics of k_c^2 (the eigenvalues of the chaotic modes) and $\phi_c(\vec{x})$ (the corresponding eigenmodes). The distribution of k_c^2 is taken to be the same as that of the eigenvalues of a random matrix with same mean spacing $\Delta_C = \langle k^2_{c+1} - k^2_c\rangle = 4\pi/A_C$. Using Eq. (28), we can calculate the equivalent chaotic area of the mushroom cavity,

$$A_C = \frac{\sqrt{3}}{2}\rho_0^2 + \frac{1}{2}\left[\rho_0\sqrt{R^2 - \rho_0^2} + R^2 \arcsin\left(\frac{\rho_0}{R}\right)\right]. \tag{37}$$

To develop a random coupling model in a mixed system, we need to rewrite Eq. (23) as

$$\Phi_n = \mathbf{Q}\mathbf{w}_n, \tag{38}$$

where $\mathbf{Q}$ is a $M \times M$ diagonal matrix, which describes the classical chaotic probability at each port

$$Q^2_{ii} = \int_\Omega u_i(\vec{x})\sigma^2(\vec{x})d^2\vec{x}, \tag{39}$$

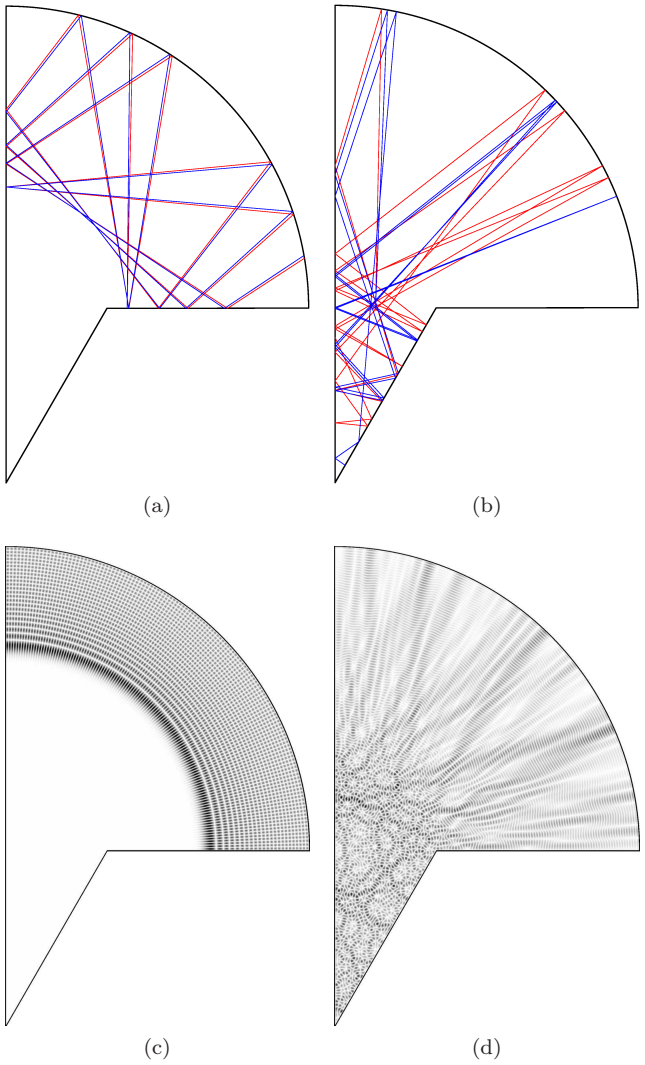

FIG. 2. (a) Two regular orbits with slightly different initial conditions. (b) Two chaotic orbits with slightly different initial conditions. (c) Magnitude squared of the $n \approx 10,002$-th eigenmode (regular) and $k_n \approx 253.496413$. (d) $n \approx 10,003$-th eigenmode (chaotic) and $k_n \approx 253.501722$.

where $\sigma(\vec{x})$ has been defined in Eq. (31). Thus in the case where all transmission lines are identical, the chaotic contribution to the impedance matrix (29c) can be written

$$Z_{C,ij}(k^2) = j\frac{kh\eta_0}{4} A_C Q_{ii} Q_{jj} \Xi_{ij}. \tag{40}$$

Figures 2(c) and 2(d), respectively, show representative, numerically computed, regular and chaotic eigenfunctions. These figures and others (not shown) demonstrate that, consistent with Percival's conjecture [23], the eigenfunctions concentrate either in the regular or chaotic phase space regions thus justifying the decomposition (29). We next test the statistics predicted by Eq. (40) by comparison with direct numerical computations on our mushroom billiard example.

III. NUMERICAL EXPERIMENT

In order to test our theory for the impedance in mixed system, we numerically solve the Helmholtz equation for its eigenfunctions and eigenenvalues to calculate Eq. (29) and compare with our statistical model, Eqs. (36) and. (40). We use about 10,000 eigenmodes for the sum in Eq. (16). For our numerical eigenmode solutions, we use the scaling method introduced by Vergini and Saraceno [19, 28] which facilitates relatively fast solutions. It has already been shown that this method yields accurate results for the eigenmodes of the Mushroom billiard [26]. We use $\alpha = 3/4$ (see Fig. 1(a)) rather than the value $\alpha = 2/3$ employed in Ref. [26], in order to allow application of Steed's Method [29] for efficient evaluation of the Besssel function.

After solving for all eigenmodes, we classify these eigenfunctions by examining the magnitude of their normal derivative as a function of the boundary coordinate s (see Fig. 3). By this means we can associate all our numerically calculated regular eigenmodes with one of the analytically predicted approximate eigenmodes (32). Moreover, we have also compared the regular eigenfunctions and eigenenvalues determined by our numerical solutions with the approximate analytic solutions; they agree well. Thus, the regular contribution to the impedance matrix (29b) is very well-approximated by Eq. (36) with our approximate analytic regular eigenfunctions (32). [Alternatively, one can also characterize the regular contribution to $\mathbf{Z}$ in a more universal manner, independent of specific geometry, as described in Appendix A.]

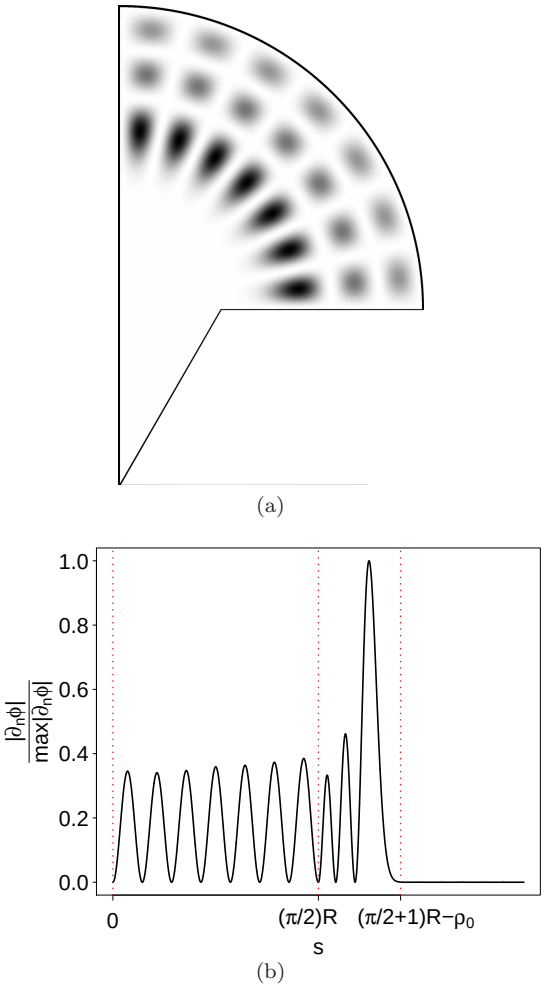

FIG. 3. (a)Regular eigenmode, $\phi_{14,3}(\vec{x})$, in Ω. (b)Corresponding magnitude of the normal derivative of $\phi_{14,3}(\vec{x})$versus s.

Our first goal is to test our statistical model for the chaotic contribution to $\mathbf{Z}_C = \mathbf{Z} - \mathbf{Z}_R$, where our model requires only simple system information (cavity area, phase space distribution) rather than all numerical eigenfunctions. For simplicity, we choose all ports to be identical, uncorrelated and point-like, i.e., $u_i(\vec{x}) = \delta(\vec{x} - \vec{x}_i)$; thus, $Q_{ii} = \sigma(\vec{x}_i)$ and Eq. (16) becomes

$$Z_{ij}(k^2) = jkh\eta_0\xi_{ij}(k^2), \tag{41}$$

where

$$\xi_{ij}(k^2) = \sum_{n=1}^{N} \frac{\phi_n(\vec{x}_i)\phi_n(\vec{x}_j)}{k^2 - k_n^2}, \tag{42}$$

and we similiarly define ξ_C and ξ_R.

We choose the cutoff $N_C = N \times A_C/A = 2k^2/\Delta_C$. With this definition, the expectation value of

$$\xi_{C,ij}(k^2) = \sum_{c=1}^{2k^2/\Delta_C} \frac{\phi_c(\vec{x}_i)\phi_c(\vec{x}_j)}{k^2 - k_c^2}, \tag{43}$$

is zero since we expect equal number of k_c^2 such that $k_c^2 > k^2$ and $k_c^2 < k^2$. Our goal is to find the probability density functions of $\xi_{C,ij}$ if we randomly choose a k^2 (see Fig. 4).

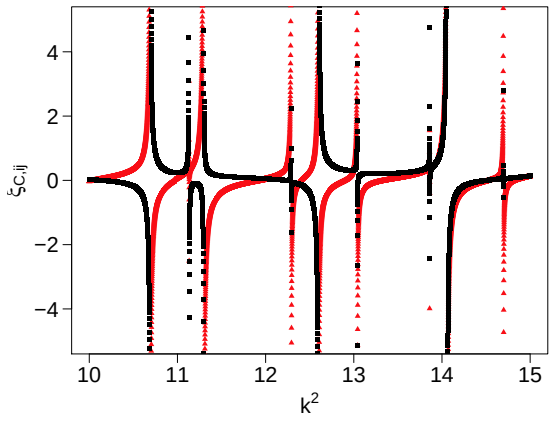

FIG. 4. Numerical calculation of $\xi_{C,ii}$ (red triangle) and $\xi_{C,ij}$ (black square) in the mushroom cavity vs. energy (k^2).

We use a Monte Carlo method to generate realizations of Eq. (43). In each realization, we generate

$k_1^2, k_2^2, \ldots, k_{N_C}^2$ by calculating the eigenvalues of a GOE random matrix and unfold the spectra [2] such that the mean spacing is $4\pi/A_C$; we also generate $(\phi_1(\vec{x}_i), \phi_1(\vec{x}_j)), (\phi_2(\vec{x}_i), \phi_2(\vec{x}_j)), \ldots, (\phi_{N_C}(\vec{x}_i), \phi_{N_C}(\vec{x}_j))$ according to Eqs. (30) and (31); then, we calculate $\xi_{C,ij}$ at each value of k^2; finally, we construct a probability density function for $\xi_{C,ij}$. After N_R realizations, we have N_R probability density functions for $\xi_{C,ij}$, i.e, $p_n(\xi), n = 1, \ldots, N_R$. We then calculate the mean and variance of the probability density at each ξ, i.e,

$$\bar{p}(\xi) = \frac{1}{N_R} \sum_{n=1}^{N_R} p_n(\xi), \tag{44}$$

$$\sigma_p^2(\xi) = \frac{1}{N_R} \sum_{n=1}^{N_R} \left[p_n(\xi) - \bar{p}(\xi)\right]^2. \tag{45}$$

We also calculate Eq. (43) numerically for different port positons from the numerically determined eigenfunctions and eigenvalues and compare with our statistical model Monte Carlo method (see Fig. 5). Our statistical model of impedance in different port positions is the statistical model of the same normalized impedance (Eq. (25)) with a position dependent factor, $A_C Q_{ii} Q_{jj}$, defined in Eqs. (28), (31), (39) and (40). The agreement between the numerical result and our statistical model for the different cases in Fig. 5 shows that the chaotic contribution to the impedance in a mixed system has the same statistics as the impedance in a purely chaotic system, provided one accounts for variations in the size of the chaotic portion of phase space accesible at the locations of the ports.

Our second goal is to compare the previous statistical model of ξ_{ij} in Ref. [7] (which assumes that the classical trajectories are all chaotic) with our statistical model of ξ_{ij} [which includes chaotic contributions ($\xi_{C,ij}$) and an approximated formula for regular contributions ($\xi_{R,ij}$) defined in Eq. (42)]. Figure 6 shows that our statistical model (red solid curves) predicts the probability density function of ξ_{ij} much better than the previous result (blue dashed curves) that one would obtain by supposing that the entire phase space was chaotic.

Note that, in our formulation in Eq. (32), $\phi_{mn}(\vec{x}_i) = 0$ if $\vec{x}_i$ is located in the stem of the mushroom. Therefore, if at least one port, say port i, is located in the stem of the mushroom, then $\xi_{R,ij} = 0$ and only chaotic modes contribute to the impedance, i.e., $\xi_{ij} = \xi_{C,ij}$. In the insets of Fig. 6, we show probability density functions of $\xi_{R,ij}$ calculated from numerically obtained regular eigenmodes and the probability density function of $\xi_{R,ij}$ calculated from our approximate regular eigenmodes (delta function (red) at $\xi_{R,ij} = 0$ for the insets to Figs. 6(a and b) and red curve in the inset to Fig. 6 (c)). In particular, we observe that the pdf widths in the insets to Figs. 6 (a and b) are much less than for the inset to Fig. 6(c). The small pdf widths in the insets to Figs. 6 (a and b) can perhaps be explained by dynamical tunneling (see [33, 34]); however, this effect is not significant in the probability density function of $\xi_{ij} = \xi_{R,ij} + \xi_{C,ij}$ which is the convolution of the probability density function of $\xi_{C,ij}$ and $\xi_{R,ij}$.

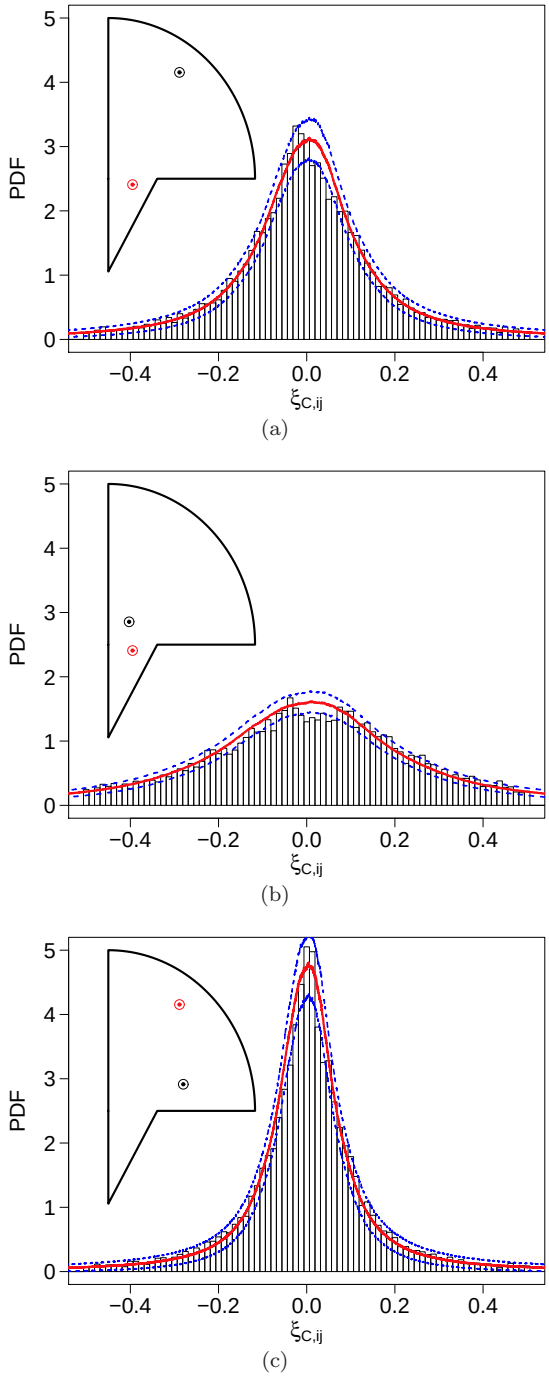

FIG. 5. Plot of the probability density function from numerical solution (black histogram) and mean probability density function from Monte Carlo simulation (red solid curve), Eq. (44), with root mean squared error bounds (blue dashed curve), Eq. (45). The black and red dots are the position of coaxial transmission lines (ports) in case (a) one port in chaotic region and the other in mixed region (b) both pots in chaotic region (c) both ports in mixed region.

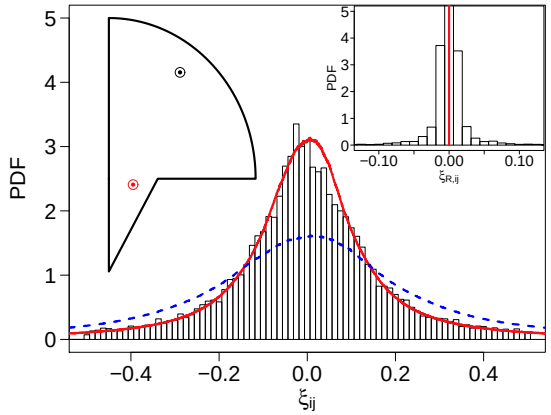

FIG. 6. Plot of the probability density function of $\xi_{ij} = \xi_{R,ij} + \xi_{C,ij}$ from numerical eigenmode solution (black histogram), our statistical model that treats regular and chaotic contributions separately (red solid curve), and previous statistical model that assumes that all eigenmodes are chaotic (blue dashed curve). The black and red dots are the position of coaxial transmission lines (ports) in case (a) one port in chaotic region and the other in mixed region (b) both pots in chaotic region (c) both ports in mixed region. The insets show the probability density function of the regular contribution, $\xi_{R,ij}$, for numerical eigenmode solutions (black histogram) and for the approximate eigenmode in Eq. (32) (red solid curve).

IV. DISCUSSION

In this paper, we develop a method for obtaining the short wavelength statistical properties of the impedance matrix of wave systems whose ray equations yield a 'mixed' phase space with coexisting chaotic and regular orbits.

In obtaining our results for the mushroom billiard, we assume that the regular eigenmodes are approximately the same as the eigenmodes in a quarter circle cavity. In formulating our theory, we have neglected the possibility that there may be some modes where the regular and chaotic phase space regions are coupled by dynamical tunneling, thus changing both the eigenfunctions and eigenenergies. These mixed modes, whose eigenfunctions show characteristic of both regular and choatic behavior, can change the wave scattering properties at k^2 near these resonances and this effect can be treated semiclassically for the particular modes under consideration. However, in our formulation, we are not interested in specific k^2 values but rather the pdf for a randomly chosen k^2 values. In our system the number of these chaos/regular mixed modes appears to be relatively small compared with modes that are predominantly confined to either the regular or the chaotic phase space regions. Thus, we expect mixed chaos/regular modes do not make a significant contribution to the mode counting formula in Eq. (27), and this expectation is confirmed by the good agreement between our numerical results and theory.

In our model, appropriate to the situation that we numerically tested, we assume that $\phi_n(\vec{x}_i)$ and $\phi_n(\vec{x}_j)$ are independent gaussian random variables for chaotic wavefunctions, which only applies if ports i and j are far apart, $k|\vec{x}_i - \vec{x}_j| \gg 1$, and both ports are not close to the cavity boundary. This assumption, however, is not essential: two-point correlations in the random wave model have been previously studied [31, 32] and can be accounted for by regarding $\phi_n(\vec{x}_i)$ and $\phi_n(\vec{x}_j)$ as correlated bivariate Gaussian random variables with a correlation that takes into account direct and indirect ray paths between $\vec{x}_i$ and $\vec{x}_j$ [35].

ACKNOWLEDGMENTS

This work was supported by ONR (grants N00014-07-1-0734 and N000140911190) and by AFOSR (grant FA99500710049).

Appendix A: Lorentzian Distribution of the Regular Normalized Impedance

Consider the normalized impedance,

$$\Xi_{ij} = -\frac{1}{\pi}\sum_{n=1}^{N}\frac{w_{ni}w_{nj}}{\tilde{k}^2 - \tilde{k}_n^2}, \tag{A1}$$

where (w_{ni}, w_{nj}) are birvariate random variables with probability density funtion (PDF) $f_{ij}(w_{ni}, w_{nj})$, and $\tilde{k}_n^2$ are independent random variables distributed uniformly on $(0, \tilde{k}_N^2)$, i.e., the PDF is $f_{\tilde{k}^2}(\tilde{k}^2) = 1/\tilde{k}_N^2$. Let

$$\xi_{n,ij} = -\frac{1}{\pi}\frac{w_{ni}w_{nj}}{\tilde{k}^2 - \tilde{k}_n^2}, \tag{A2}$$

such that

$$\Xi_{ij} = \sum_n \xi_{n,ij}. \tag{A3}$$

The PDF, $f_\Xi(z)$, and the characteristic function of Ξ, $\Phi_\Xi(t)$ are given by

$$f_\Xi(z) = \int d\xi_1 ... d\xi_N \prod_{n=1}^{N} f_\xi(\xi_n)\delta(z - \sum_{n'} \xi_{n'}), \tag{A4}$$

$$\Phi_\Xi(t) = \int d\xi_1 ... d\xi_N \prod_{n=1}^{N} f_\xi(\xi_n) \exp(it \sum_{n'} \xi_{n'}) = [\Phi_\xi(t)]^N, \tag{A5}$$

where $f_\xi(\xi_n)$ is the PDF of ξ and $\Phi_\xi(t) = \int d\xi_n \exp(it\xi_n) f_\xi(\xi_n)$ is the characteristic function of ξ. We can calculate $\Phi_\xi(t)$ by directly evaluating the integral,

$$\Phi_\xi(t) = \int dw_{ni} dw_{nj} f_{ij}(w_{ni}, w_{nj}) \times \int_0^{\tilde{k}_N^2} d\tilde{k}_n^2 \frac{1}{\tilde{k}_N^2} \exp\left(-it\frac{1}{\pi}\frac{w_{ni}w_{nj}}{\tilde{k}^2 - \tilde{k}_n^2}\right). \tag{A6}$$

For small values of t, relevant in the limit $N \gg 1$, the second integral of (A6) is

$$\begin{aligned}&\frac{1}{\tilde{k}_N^2}\int_0^{\tilde{k}_N^2} d\tilde{k}_n^2 \exp\left(-it\frac{1}{\pi}\frac{w_{ni}w_{nj}}{\tilde{k}^2 - \tilde{k}_n^2}\right)\\ =&1 + \frac{|t||w_{ni}w_{nj}|}{\tilde{k}_N^2} - it\frac{1}{\pi}\frac{w_{ni}w_{nj}}{\tilde{k}_N^2}\log\left|\frac{\tilde{k}^2}{\tilde{k}_N^2 - \tilde{k}^2}\right| + O(t^2),\end{aligned} \tag{A7}$$

which to first order in t yields

$$\begin{aligned}\Phi_\xi(t) \approx& \int dw_{ni} dw_{nj} f_{ij}(w_{ni}, w_{nj}) \\ &\times \left(1 + \frac{|t||w_{ni}w_{nj}|}{\tilde{k}_N^2} - it\frac{1}{\pi}\frac{w_{ni}w_{nj}}{\tilde{k}_N^2}\log\left|\frac{\tilde{k}^2}{\tilde{k}_N^2 - \tilde{k}^2}\right|\right)\\ =& 1 - \frac{1}{\tilde{k}_N^2}\left(-it\frac{E\{w_{ni}w_{nj}\}}{\pi}\log\left|\frac{\tilde{k}^2}{\tilde{k}_N^2 - \tilde{k}^2}\right| \right.\\ &\left. + |t|E\{|w_{ni}w_{nj}|\}\right),\end{aligned} \tag{A8}$$

where $E\{\cdots\} = \int \cdots f_{ij}(w_{ni}, w_{nj}) dw_{ni} dw_{nj}$. Now, we calculate $\Phi_\Xi(t)$; since the mean spacing between adjacent $\tilde{k}_n^2$ is normalized to unity, we can replace $\tilde{k}_N^2$ in (A8) by N and insert it into (A5). As $N \to \infty$, we obtain

$$\begin{aligned}\Phi_\Xi(t) =& \left[1 - \frac{1}{N}\left(-it\frac{E\{w_{ni}w_{nj}\}}{\pi}\log\left|\frac{\tilde{k}^2}{\tilde{k}_N^2 - \tilde{k}^2}\right| \right.\right.\\ &\left.\left. + |t|E\{|w_{ni}w_{nj}|\}\right)\right]^N\\ \to& \exp\left(it\frac{E\{w_{ni}w_{nj}\}}{\pi}\log\left|\frac{\tilde{k}^2}{\tilde{k}_N^2 - \tilde{k}^2}\right| - |t|E\{|w_{ni}w_{nj}|\}\right).\end{aligned} \tag{A9}$$

Comparing with the characteristic function of a Lorentzian RV with mode x_0 and width W, $\Phi(t) = \exp(itx_0 - W|t|)$, we know Ξ_{ij} is Lorentzian distributed with mode $E\{w_{ni}w_{nj}\}(\log|\tilde{k}^2| - \log|\tilde{k}_N^2 - \tilde{k}^2|)/\pi$ and width $E\{|w_{ni}w_{nj}|\}$. Since the spacing distribution of $\tilde{k}_n^2$ for regular systems is exponential distributed, as $N \to \infty$, the distribution of $\tilde{k}_n^2$ is uniformly distributed in $(0, N)$; thus, the normalized impedance of regular systems are also Lorentzian distributed and all the system specific informations are included in mode and width of the Lorentzian.

* leemj@umd.edu

[1] E. P. Wigner, Ann. Math. **53**, 36 (1951); **62**, 548 (1955); **65**, 203 (1957); **67**, 325.

[2] F. Haake, *Quantum Signatures of Chaos*, 2nd ed. (Springer, New York, 2000).

[3] M. C. Gutzwiller, *Chaos in Classical and Quantum Mechanics* (Springer, New York, 1990).

[4] H.-J. Stöckmann, *Quantum Chaos* (Cambridge University Press, Cambridge, England, 1999).

[5] P. A. Mello, P. Pereyra, and T. H. Seligman, Annals of Physics **161**, 254 (1985); P. W. Brouwer, Phys. Rev. B **51**, 16878 (1995); D. V. Savin, Y. V. Fyodorov, and H.-J. Sommers, Phys. Rev. E **63**, 035202 (2001); R. A. Méndez-Sánchez, U. Kuhl, M. Barth, C. H. Lewenkopf, and H.-J. Stöckmann, Phys. Rev. Lett. **91**, 174102 (2003).

[6] U. Kuhl, M. Martínez-Mares, R. A. Méndez-Sánchez, and H.-J. Stöckmann, Phys. Rev. Lett. **94**, 144101 (2005).

[7] X. Zheng, Ph.D. thesis, University of Maryland (2005); T. M. Antonsen X. Zheng and E. Ott, Electromagnetics **26**, 3 (2006); **26**, 37 (2006).

[8] E. Doron, U. Smilansky, and A. Frenkel, Phys. Rev. Lett. **65**, 3072 (1990).

[9] P. W. Brouwer and C. W. J. Beenakker, Phys. Rev. B **55**, 4695 (1997).

[10] S. Hemmady, X. Zheng, E. Ott, T. M. Antonsen, and S. M. Anlage, Phys. Rev. Lett. **94**, 014102 (2005).

[11] L. A. Bunimovich, Chaos **11**, 802 (2001).

[12] More generic systems can display infinite hierarchies of KAM island chains encircling other KAM island chains with chaos intermixed (e.g., J. D. Meiss and E. Ott, Phys. Rev. Lett. **55**, 2741 (1985)). This type of intermingling of chaotic and nonchaotic orbits on all scales is not present in the mushroom billiard where non-smooth shape is designed to yield a clear division between chaotic and regular phase space region. Our motivation in using the mushroom shape is that the simplicity provided by its clear division of chaotic and regular phase space allows a potentially simpler theory. We hope that our work can serve as a basis for future study applicable to the case of generic phase space structure

[13] M. V. Berry and M. Robnik, Journal of Physics A: Mathematical and General **17**, 2413 (1984).

[14] O. Bohigas, S. Tomsovic, and D. Ullmo, Phys. Rep. **223**, 43 (1993).

[15] T. Prosen and M. Robnik, Journal of Physics A: Mathematical and General **26**, 5365 (1993); B. Li and M. Robnik, **28**, 4843 (1995).

[16] Y.-C. Lai, R. Blümel, E. Ott, and C. Grebogi, Phys. Rev. Lett. **68**, 3491 (1992).

[17] R. Ketzmerick, Phys. Rev. B **54**, 10841 (1996).

[18] A. M. Chang, H. U. Baranger, L. N. Pfeiffer, and K. W. West, Phys. Rev. Lett. **73**, 2111 (1994).

[19] A. H. Barnett, Commun. Math. Phys. **59**, 1457 (2006).

[20] H. Weyl, Nachr. Akad. Wiss. Göttingen, 110(1911).

[21] E. Ott, *Chaos in Dynamical Systems*, 2nd ed. (Cambridge University Press, Cambridge, England, 2002).

[22] M. V. Berry, J. Phys. A: Math. and Gen. **10**, 2083 (1977).

[23] I. C. Percival, J. Phys. B: Atom. and Mol. **6**, L229 (1973).

[24] A. Bäcker, R. Ketzmerick, S. Löck, and H. Schanz, Eur. Phys. J. **94**, 30004 (2011).

[25] A. Bäcker and R. Schubert, J. Phys. A: Math. and Gen. **35**, 527 (2002).

[26] A. H. Barnett and T. Betcke, Chaos **17**, 043125 (2007).

[27] R. W. Robinett, Am. J. Phys. **64**, 440 (1996).

[28] E. Vergini and M. Saraceno, Phys. Rev. E **52**, 2204 (1995).

[29] A. Barnett, D. Feng, J. Steed, and L. Goldfarb, Comput. Phys. Commun. **8**, 377 (1974).

[30] E. J. Heller , Phys. Rev. Lett. **53**, 1515 (1984).

[31] Urbina, J. D. and Richter, K., Eur. Phys. J. Special Topics **145**, 255 (2007).

[32] M. Srednicki, Phys. Rev. E **54**, 954 (1996).

[33] B. Dietz, T. Friedrich, M. Miski-Oglu, A. Richter, and F. Schäfer, Phys. Rev. E **75**, 035203 (2007).

[34] A. Bäcker, R. Ketzmerick, S. Löck, M. Robnik, G. Vidmar, R. Höhmann, U. Kuhl, and H.-J. Stöckmann, Phys. Rev. Lett. **100**, 174103 (2008).

[35] S. Hortikar and M. Srednicki, Phys. Rev. Lett. **80**, 1646 (1998).